Sonoelastographic imaging of interference patterns for estimation of the shear velocity of homogeneous biomaterials

Zhe Wu[1], Lawrence S Taylor[2], Deborah J Rubens[3] and Kevin J Parker[1]

[1] ECE Department, University of Rochester, Hopeman Building 204 Rochester, NY 14627-0126, USA
[2] BME Department, University of Rochester, Rochester, NY 14627-0126, USA
[3] Department of Radiology, University of Rochester, Rochester, NY 14627-0126, USA

E-mail: wuzhe@ece.rochester.edu

Abstract

The shear wave velocity is one of a few important parameters that characterize the mechanical properties of bio-materials. In this paper, two noninvasive methods are proposed to measure the shear velocity by inspecting the shear wave interference patterns. In one method, two shear wave sources are placed on the opposite two sides of a sample, driven by the identical sinusoidal signals. The shear waves from the two sources interact to create interference patterns, which are visualized by the vibration sonoelastography technique. The spacing between the pattern bands equals half of the shear wavelength. The shear velocity can be obtained by taking the product of the wavelength and the frequency. An alternative method is to drive the two vibration sources at slightly different frequencies. In this case, the interference patterns no longer remain stationary. It is proved that the apparent velocity of the moving patterns is proportional to the shear velocity in the medium. Since the apparent velocity of the patterns can be measured by analysing the video sequence, the shear velocity can be obtained thereafter. These approaches are validated by a conventional shear wave time-of-flight approach, and they are accurate within 4% on various homogeneous tissue-mimicking phantoms.

1. Introduction

It is well known that many diseases are associated with some sort of change in the mechanical properties of bio-tissues (Tumen and Cohn 1965, Fentiman 1997). Physicians have long used manual palpation as a screening method in physical examinations (Carvalhal *et al* 1999, Obek *et al* 1999). When doing so they are making a qualitative assessment of the shear

stiffness (modulus) of the tissue. One way of quantifying the change is to measure the shear velocity in the tissue (Vexler *et al* 1999). In a linear elastic medium the shear modulus is equal to the square of the shear velocity times the density (Love 1944, Achenbach 1973a). When the tissue is better characterized as a linear viscoelastic medium, the shear modulus will be complex and the shear velocity may exhibit frequency dispersion (Achenbach 1973b).

Yamakoshi *et al* (1990) developed an approach to measure shear velocity. External low frequency vibration was applied to the region of interest, then both amplitude and phase of the vibration were mapped using a Doppler detection technique. The vibration phase image was used to measure the wave propagation velocity. It was found that refraction and reflection of the propagating vibration waves at internal tissue boundaries can create bias in the phase map. Standing waves whose wavelength differs from that of the shear wave propagation can occur.

Magnetic resonance imaging (MRI) has also been applied to this problem. Muthupillai *et al* (1995) sensitized a gradient-echo imaging pulse to harmonic motion permitting them to generate a MRI phase image which allowed measurement of wavelength among other properties. Bishop *et al* (1998) applied this technique to the problem of visualizing shear wave propagation in excised tissue samples. Later, Smith *et al* (1999) proposed a method to filter out the other modes of motion such as reflections, vibrations and ambient background motions that sometimes obscure the accurate measurement of the shear waves when using this technique.

Catheline *et al* (1999) proposed an ultrasound technique, which they call transient elastography, to deal with some of artefact issues caused by wave reflection and standing waves. This method uses a low-frequency transient vibration to create displacements in tissue, which are then detected using pulse echo ultrasound. Ultrasonic A-lines (oscilloscope traces of the echo amplitude along the wave propagation of the ultrasound pulses) are collected at the frame rate of 1300 Hz immediately before and during the application of a low frequency (40–250 Hz) tone burst vibration to a 6% gel phantom. Cross correlation techniques are then used between successive A-lines to estimate the particle displacement during the period the shear waves are propagating but before any boundaries are reached. This avoids problems with standing waves. The shear wavelength can be estimated from the visualized wave progression. This technique is effective but requires frame rates exceeding those of available ultrasound scanners. Dutt *et al* (2000) developed an ultrasonic method of visualizing shear wave propagation and compared it to the MRI based technique. A-lines were collected at 5 to 10 kHz in synchronism with low frequency (200 to 500 Hz) 20–25 ms tone bursts from a speaker coil. Using this technique they were able to both visualize shear wave propagation and measure shear velocity.

Nightingale *et al* (2003) have developed an ultrasonic method of visualizing shear wave propagation involving mechanical excitation of the tissue with acoustic radiation force. A repeated interrogation approach was used to get around the necessity of using high frame rates to adequately sample the region of interest. Shear waves were generated by the radiation force and both high quality shear wave image sequences (movies) and the measurement of shear velocity was achieved using a modified commercially available ultrasound scanner.

The potential clinical significance of measuring the shear wave velocity is illustrated in a recent paper by Sanada *et al* (2000). Sanada and co-workers have applied an ultrasound approach to the problem of measuring the mechanical properties of the liver which they call sonoelasticity. A low frequency (40 Hz) vibration source was used to propagate shear waves in human liver *in vivo* while an ultrasound Doppler signal detection technique was used to estimate the wavelength of the propagating shear waves, the shear velocity being inferred from the wavelength. This method was used to measure the shear velocity in the livers of

45 normal volunteers, 153 patients with liver cirrhosis and 83 patients with chronic hepatitis. In the mean, the measured velocity in patients with liver cirrhosis was twice that measured in the healthy volunteers. This implies that shear velocity is a specific indicator of diffuse liver disease such as cirrhosis.

In this paper, new techniques are introduced to measure the wavelength and velocity of shear waves in bio-materials. In these techniques, two shear wave sources are placed on either side of a region of interest. When the sources are vibrated in phase at the same frequency the resulting interference pattern, when visualized by sonoelastography imaging, shows stationary peaks and troughs which are located at intervals equal to half the shear wavelength. Furthermore, when the sources are vibrated at slightly different frequencies the interference pattern moves from the higher frequency source to the lower frequency source. This apparent motion, which might be termed a 'crawling wave' (i.e. falling between travelling and standing waves), is shown to have a velocity which depends directly on the shear velocity but is scaled by a certain ratio of the frequency difference to twice of the frequency of the lower source. This can effectively slow down the shear waves by one or two orders of magnitude, allowing commercially available ultrasound systems to be used for imaging. We experimentally validate these methods by comparing our results to conventional time-of-flight experiments which are described in the literature (McAleavey *et al* 1999, Vexler *et al* 1999). The results are shown to be accurate within 4% on various homogeneous tissue-mimicking phantoms.

2. Theory

2.1. Basic theory

It is well accepted that the speed of the shear wave propagation in a linear elastic medium is directly related to the mass density ρ and the shear modulus G of the medium.

$$v_{\text{shear}} = \sqrt{\frac{G}{\rho}}. \tag{1}$$

Therefore, the shear modulus G can be determined by measuring the speed of the shear waves and the density, provided that the medium is homogeneous and isotropic. By noting the identity that $v_{\text{shear}} = f * \lambda$, the shear modulus can be calculated once the shear wavelength is measured and all the other parameters are known: $G = \rho \cdot (f \cdot \lambda)^2$.

2.2. Sonoelastography

The methods we propose are based on an ultrasonic imaging modality called sonoelastography (Lerner *et al* 1988). Sonoelastography measures and images the peak displacement of the audio frequency local particle motion by analysing the Doppler variance of the ultrasound echoes (Huang *et al* 1990, Taylor *et al* 2000). From the signal processing perspective, sonoelastography visualizes the envelope signal of the particle motion. Vibration fields are mapped to a commercial ultrasound scanner's screen in real time. Regions where the vibration amplitude is low are shown as dark green, while regions with high vibration are shown as bright green. Since the phase data are lost while displaying the vibration amplitude, sonoelastography does not display the shear wavelength, unless additional phase estimators are employed (Huang *et al* 1992). Sonoelastography has been applied to visualize the shear wave transducers' beam patterns or interference patterns (Wu *et al* 2002).
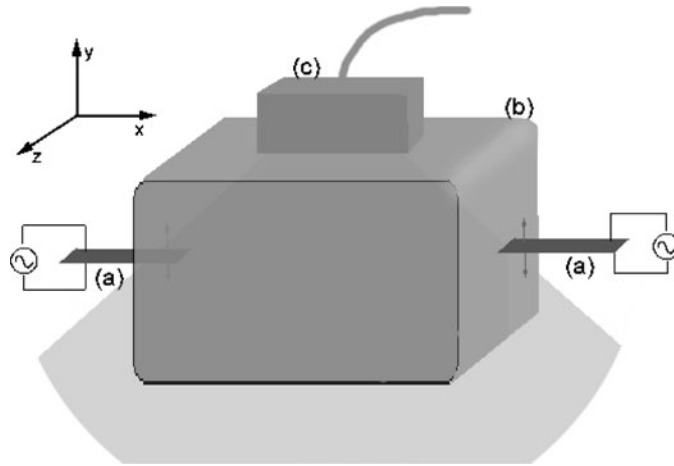
Figure 1. Schematic drawing of the experiment set-up. Two bimorphs (a) are in close contact with the phantom (b). The arrows indicate the motion vectors of the tips of the bimorphs. The sector shape depicts the imaging plane of the ultrasound probe (c).
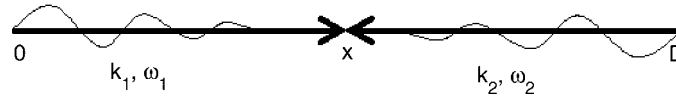

Figure 2. Coordinate system for equations (2) and (3). The right travelling and the left travelling shear waves from two sources are depicted. Two sources locate at 0 and D, respectively. In the static pattern case, $k_1 = k_2 = k$ and $\omega_1 = \omega_2 = \omega$. In the moving pattern case, $k_2 = k_1 + \Delta k = k + \Delta k$ and $\omega_2 = \omega_1 + \Delta\omega = \omega + \Delta\omega$.

2.3. Static interference pattern estimates

In order to measure the wavelength of the propagating shear waves, we propose to apply two vibration sources of identical frequencies and amplitudes. The two sources are placed on opposite sides of the testing sample. The tip of each source oscillates along a vector parallel to the surface of the sample. The imaging plane is defined by the two vibration sources and the ultrasonic probe. Since sonoelastography only images the particle motion along the ultrasound beam, which is roughly in y direction, only the y component of the wave motion will be discussed in this paper. Please see figure 1 for illustration. The waves from one of the sources interact with the waves from the other source to create an interference pattern. The pattern is mainly determined by the wavelength and the signal frequency. In the homogeneous medium, if the two vibration sources are relatively far away from the region of interest (ROI), each train of waves can be considered as plane waves, and the interference patterns appear as parallel stripes. The stripes are perpendicular to a line connecting the two vibration sources. Under the plane wave assumption, it is proved as follows that the spacing between the parallel stripes is half of the shear wave wavelength. As illustrated in figure 2, considering two plane wave sources with separation D. The right travelling shear waves can be expressed as

$$\exp(ikx - i\omega t).$$

The left travelling shear waves can be expressed as

$$\exp(ik(D - x) - i\omega t).$$

The interference patterns are the superposition of the two waves

$$\exp(\mathrm{i}kx - \mathrm{i}\omega t) + \exp(\mathrm{i}k(D - x) - \mathrm{i}\omega t)$$

where k is the shear wave number $k = \frac{\omega}{v_{\mathrm{shear}}}$ and ω is the angular frequency $\omega = 2\pi f$.

Take only the real part of the terms

$$u(x, t) = \cos(kx - \omega t) + \cos(kD - kx - \omega t)$$
$$= 2\cos\left(kx - \frac{kD}{2}\right) * \cos\left(\omega t - \frac{kD}{2}\right) \tag{2}$$

where u is the vibration amplitude.

The second term is spatially invariant and it is not imaged by sonoelastography. The first term, however, is time invariant and has a spatial distribution. Recall that sonoelastography images the *peak* value of the vibration field, thus the image actually becomes $\left|2\cos\left(kx - \frac{kD}{2}\right)\right|$. The spatial period of this expression is $\frac{\lambda}{2}$, where λ is the wavelength of the shear wave. Thus, the shear wave wavelength can be calculated as twice the spacing between the interference patterns. The shear wave speed can be obtained thereafter, since the signal frequency is known.

This approach is referred to as the static interference pattern approach.

2.4. Moving pattern estimates

As an alternative approach, if one of the two driving signals is tuned to be slightly different from the other signal, for example, signal A is a sinusoidal function at frequency ω and signal B is at frequency $\omega + \Delta\omega$, the interference patterns are no longer static. The patterns will then move towards the source with the lower frequency. This phenomena may be termed as 'crawling waves'. Under plane wave assumption, the relation between the apparent speed of the crawling waves and the true shear wave speed can be deduced as follows.

The right travelling waves can be expressed as

$$\exp(\mathrm{i}kx - \mathrm{i}\omega t).$$

The left travelling waves can be expressed as

$$\exp[\mathrm{i}(k + \Delta k)(D - x) - \mathrm{i}(\omega + \Delta\omega)t]$$

where

$$\Delta k = \frac{\Delta\omega}{v_{\mathrm{shear}}}.$$

The interference patterns are the superposition of the two waves

$$\exp(\mathrm{i}kx - \mathrm{i}\omega t) + \exp[\mathrm{i}(k + \Delta k)(D - x) - \mathrm{i}(\omega + \Delta\omega)t].$$

Take only the real part of the terms

$$u(x, t) = \cos(kx - \omega t) + \cos((k + \Delta k)(D - x) - (\omega + \Delta\omega)t)$$
$$= 2\cos\left[\left(k + \frac{\Delta k}{2}\right)x + \frac{\Delta\omega}{2}t\right] * \cos\left[\frac{\Delta k}{2}x + \left(\omega + \frac{\Delta\omega}{2}\right)t\right]. \tag{3}$$

Note that D merely introduces a constant phase and is thus omitted for simplicity.

Equation (3) factorizes the two waves into rapidly varying carrier signals (the second factor) and slowly varying envelope signals (the first factor). Since sonoelastography only images the envelope, it is the absolute value of the first factor that is displayed. Also note that there are both time variables and spatial variables in this factor. It appears to be a

travelling wave. The *apparent* speed of these 'crawling waves' can be derived by using: $v_{\text{pattern}}^2 = \frac{\partial^2 u}{\partial t^2} / \frac{\partial^2 u}{\partial x^2}$, thus

$$v_{\text{pattern}} = \frac{\Delta\omega}{2\left(k + \frac{\Delta k}{2}\right)}. \tag{4}$$

It is interesting to analyse two mathematical extremes of equation (4). Firstly, if we keep one of the sources vibrating and completely mute the other source, that is let k be 0 and Δk be large, $v_{\text{pattern}} = \frac{\Delta\omega}{\Delta k} = v_{\text{shear}}$. Even though sonoelastography is not able to image the shear wave propagation in this extreme scenario, the result shows that equation (4) is mathematically justified. The other extreme is that if the frequency difference $\Delta\omega$ is small compared to ω, then Δk is small comparing to k. Therefore, $v_{\text{pattern}} \approx \Delta\omega/2k$. This is the typical configuration we use for our experiments. Noting that the speed of the shear wave is $v_{\text{shear}} = \omega/k$, the relation between the speed of the *crawling waves* and the true shear waves is

$$v_{\text{pattern}} \approx \frac{\Delta\omega}{2\omega} v_{\text{shear}} \tag{5}$$

given

$$\Delta\omega \ll \omega.$$

According to equation (5), the shear waves can be 'slowed down' one or two orders of magnitude by choosing $\Delta\omega$ much smaller than ω, so that a conventional ultrasonic scanner modified for sonoelastography can visualize and track the wave propagation. In practice, $\Delta\omega$ is normally chosen between $\omega/200$ and $\omega/100$ for the convenience concerning the ultrasonic scanner's frame rate. Once the apparent speed of the 'crawling waves' is measured by analysing the video sequences, the true shear wave speed can then be obtained from the above equation.

This method is referred to as the moving pattern approach.

3. Method and materials

In the static or moving interference pattern experiment, two bending piezo elements known as bimorphs (Piezo systems, Cambridge, MA, USA) are applied as the vibration sources. A signal generator (Tektronix FG5010) produces monochrome low frequency signals. In the moving pattern experiment, another signal generator produces the second signal. The signals pass through a two channel amplifier before fed into the bimorphs. A GE Logiq 700 which has been specially modified to realize the sonoelastography functions is applied to visualize the 'crawling wave' propagation.

In the conventional shear wave time-of-flight measurement, one bimorph is used as the transmitter and the other as the receiver. When manually triggered, a single cycle sinusoidal signal (tone burst signals where the number of burst equals one) is generated from the Textronix signal generator, feeding into an oscilloscope as channel one and into an amplifier simultaneously. When amplified, the signals drive the transmitting bimorph to send a shear wave pulse into the testing sample. The receiving bimorph picks up the signal when the shear wave pulse travels to the receiving end and feeds the signal into the oscilloscope as channel two. The receiving bimorph is held by a 3D positioner (Velmex, Bloomfield, NY) so the distance between the transmitter and the receiver is precisely controlled and measured. The time lag between pulses displayed on channel one and channel two is the time that the shear waves spend to travel from the tip of the transmitter to the tip of the receiver. Figure 3 is a schematic of the set-up of the shear wave time-of-flight experiments.
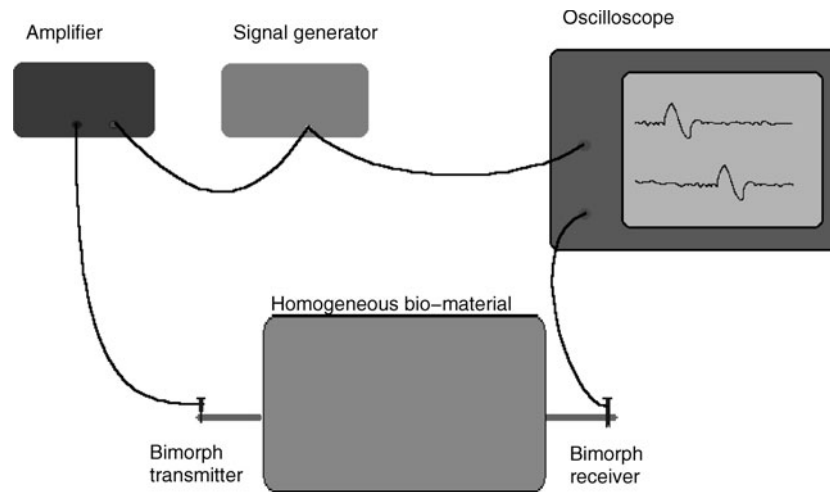
Figure 3. Schematic drawing of the transient shear wave speed measurement. The time lag between the two signals indicates the shear wave time-of-flight.

Figure 4. Sonoelastography image of shear wave interference pattern on GE Logiq 700. The medium is 5% gelatin phantom. Both sources vibrate at 200 Hz. The peak vibration amplitude in the direction of the ultrasound wave is mapped to a grey scale.

Two gelatin phantoms, both $8 \times 9 \times 12$ cm^3 in size and rectangular solids in shape approximately, are constructed for the experimental verification of the theory. The phantoms are made from 800 ml degassed, deionized water, 5% and 10% (by weight) food gelatin (Knoxx), respectively, and 10% formaldehyde (v/v), 10% glycerol (v/v) and 0.5% graphite powder as scatterers. The manufacturing procedure is described as follows. The water is first heated to boiling and then placed on the stirring plate, with a magnetic rod stirring the water. Gelatin is slowly added to the water. After all gelatin has been added, the solution is reheated to boiling in a microwave oven for 2 min with plastic wrap covering the container. Then the graphite power is mixed into the solution. The mixture is cooled for about 50 min while stirring. Finally the formaldehyde and the glycerol are mixed into the solution. A bowl-shaped
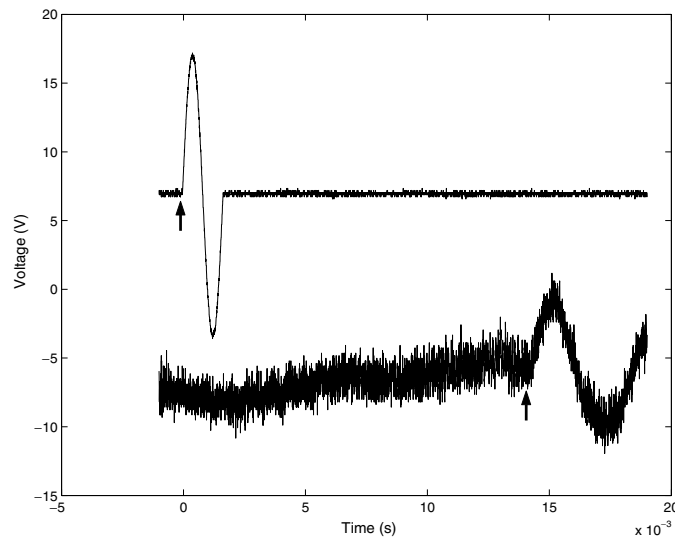
Figure 5. Example of shear wave time of flight experiment wave forms. The top wave form is the transmitted signal. The bottom waveform is the 300 times amplified received signal. The arrows indicate the transmitting time and the receiving time of the start of the pulse disturbance. The time difference between the two arrows is 14.74 ms.

Zerdine tissue phantom with stiff inclusions (CIRS Norfolk, VA) is also employed to verify that the proposed methods work on various materials and shapes.

4. Results

4.1. Pattern results

On the 5% gelatin phantom, two 'static pattern' experiments were conducted at 180 Hz and 200 Hz (figure 4). We make multiple measurements of the spacing between the pattern stripes. The shear wave wavelength is then twice of the arithmetic average of the measurements. The product of the wavelength and the signal frequency yields the shear wave speeds. The speed results of the two trials are 1.39 m s^{-1} and 1.40 m s^{-1} respectively. To perform the 'moving pattern' measurement, one of the two sources is driven by 200 Hz sinusoidal signals, the other by 200.1 Hz. An external device (VXM controller, Velmex) is programmed to trigger the ultrasound scanner at precisely 0.5 s intervals, for a total of 60 frames. The 'moving pattern' is then tracked manually. The speed of shear wave is obtained to be 1.44 m s^{-1} by applying equation (5).

On the 10% gelatin phantom, two 'static pattern' experiments were conducted at 450 Hz and 500 Hz. Because the shear wavelengths in 10% gelatin phantom are much longer than those in 5% phantoms, relatively high frequencies are chosen to have reasonable number of interference patterns in the ROI. The speed results of the two trials are 5.50 s^{-1} and 5.46 m s^{-1}, respectively. In the 'moving pattern' measurement, the two sources vibrate at 400 Hz and 400.4 Hz, respectively. The measured result is 5.43 m s^{-1}.

4.2. Shear wave time of flight results

In the shear wave time of flight experiment, the bimorphs are held tight against the surface of the gelatin phantoms. The distance between the tips of the bimorphs is measured as 81.1 mm

Table 1. Summary of shear wave speed measurements of 5% gelatin phantom with different experiment approaches.

Test type	Frequency (Hz)	Speed of shear wave (m s^{-1})
Static pattern approach	180	1.39
Static pattern approach	200	1.40
Moving pattern approach	200–200.1	1.44
Time of flight	200	1.40
Time of flight	300	1.39

Table 2. Summary of shear wave speed measurements of 10% gelatin phantom with different experiment approaches.

Test type	Frequency (Hz)	Speed of shear wave (m s^{-1})
Static pattern approach	450	5.50
Static pattern approach	500	5.46
Moving pattern approach	400–400.4	5.43
Time of flight	500	5.43

on the 5% phantom and 80.0 mm on the 10% phantom. When manually triggered, one cycle of 200 Hz pulse is transmitted into the 5% phantom through the transmitting bimorph. The time lag between the received signal and the transmitted signal is measured as 57.7 ms. One cycle of 500 Hz signal is transmitted into the 10% phantom and the time lag, as demonstrated in figure 5, is measured as 14.74 ms. The speed of shear wave is then calculated as 1.40 m s^{-1} in the 5% phantom and 5.43 m s^{-1} in the 10% phantom, respectively.

The results are summarized in tables 1 and 2. Taking the shear wave time-of-flight results as the gold standard, the error in the shear wave velocity measurement on the 5% gelatin phantom is less than 4% and the error on the 10% gelatin phantom is less than 2%.

4.3. Shear modulus

In order to estimate the shear modulus of the gelatin phantoms, we assume it can be approximated as a linear elastic material. Thus, the shear modulus $G = \rho * v^2$, where ρ is the density of the material. Taking 1.05 g cm^{-3} as the density of both phantoms, the 5% and the 10% gelatin phantoms' shear moduli are 2.07 kPa and 30.9 kPa, respectively.

5. Discussion

As shown by the experiments, when both of the bimorphs are driven by the external source, the interference between the two sources is the predominant cause of patterns. The modal patterns, which are the interference between the travelling waves and the reflected waves, are overshadowed, because the reflected waves tend to be weaker than the incident waves from the other source due to the attenuation, even though they are present. Therefore, the interference patterns, unlike the modal patterns, depend little on the shape of the phantom and the boundary conditions. Changing the phantom shape does not affect the accuracy of the measurement. An experiment on a bowl-shaped Zerdine phantom yields very similar interference patterns as observed in rectangular gelatin phantoms.

In the experiments, we observe that since a few pattern stripes are required to conduct the wavelength measurement, generally there exists in practice a frequency lower limit, which
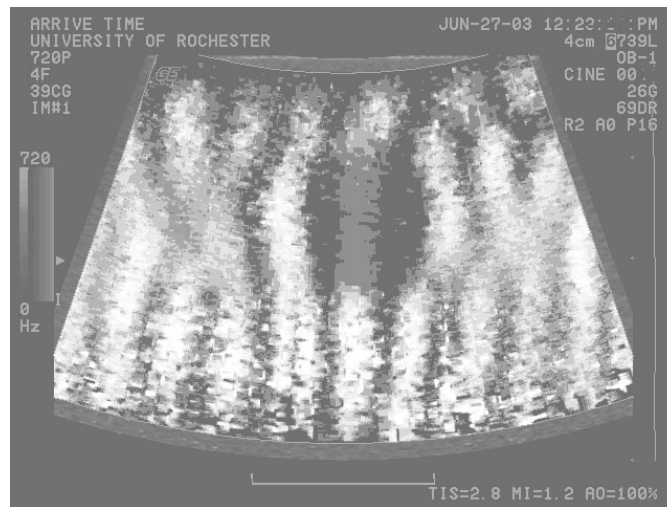
Figure 6. Sonoelastography image of shear wave interference pattern on a Zerdine phantom with a lesion in it. Both sources vibrate at 250 Hz. The image is 'histogram equalized' to enhance the visibility of details.

depends on the material property and the imaging field area. Below this frequency limit, the shear wavelength may be so long that only one or less wavelength appears in the imaging field. The measuring result in this case is ambiguous. Since the materials' shear wave attenuation usually increases while the frequency increases, there exists a frequency upper limit for the proposed techniques to be practical. Above this frequency limit, the shear wave attenuation may be so high that the two trains of waves do not meet before their energy dies out. For example, on the 5% gelatin phantom, the empirical frequency window extends from 80 Hz to 800 Hz, approximately. Within this frequency window, the precision of the technique is limited predominately by the imaging noise and resolution, as these limit the precision of estimation of the spacing between interference patterns.

Even though we focus on the measurement of shear wave velocity in homogeneous media in this paper, the techniques we propose may have foreseeable potentials to be extended into inhomogeneous cases. Some preliminary experiments have been performed on a Zerdine phantom with a stiff inclusion in it. Figure 6 shows the interference pattern image over the lesion. The pattern spacing inside the lesion appears larger than the pattern spacing outside of the lesion, indicating that the shear wave velocity is higher inside the lesion. Please note that since the interference pattern appears darker in the stiff lesion due to sonoelastography effect (Lerner *et al* 1988), figure 6 is 'histogram equalized' to enhance the visibility of the details with in the lesion. Precise shear wave velocity inversion based on the static pattern images and the moving pattern videos will be investigated in the future.

In sonoelastography, the vibration amplitude is quantized into 16 levels due to the current hardware implementation. In typical experiment procedures, the peak vibration in the FOI is adjusted to the high end of the 16 levels (just before sampling aliasing occurs), while the noise strength is usually around 1. Therefore, the signal to noise ratio (SNR) of sonoelastography is usually around 16:1. However, the SNR may be reduced in the stiff inclusions because of the decrease of the vibration amplitudes. Empirically, in the static pattern experiments, the stiff inclusions have to be larger than half of the shear wavelength which is the spacing between patterns, to be revealed. In the crawling wave experiments, the image resolution depends on the ability to track the crawling wave in the presence of noise. This problem resembles the

problem of estimating the displacement of an envelope signal, which is bounded by noise and bandwidth or time width considerations. The overall image contrast and resolution may be a combination of all the stated concerns, and the detailed analysis is beyond the scope of this paper.

6. Conclusion

Two novel approaches are proposed and evaluated for the measurement of shear wave speed in homogeneous bio-materials. Two vibration sources instead of one are utilized in these two approaches. Under sonoelastography, the interference patterns between the two wave sources reveal the phase data of shear wave propagations and thus the shear properties of the materials. In these two methods, shear wave velocity can be measured with appropriately modified commercial ultrasound scanners in real time. Both methods are validated against the previously reported shear wave time-of-flight method on various bio-materials. The maximum error on various phantoms is less than 4%.

Acknowledgment

References

Achenbach J D 1973a *Wave Propagation in Elastic Solids* (Amsterdam: North Holland New York: Elsevier) chapter 4
Achenbach J D 1973b *Wave Propagation in Elastic Solids* (Amsterdam: North Holland New York: Elsevier) section 10.5
Bishop J, Poole G, Leitch and Plewes D B 1998 Magnetic resonance imaging of shear wave propagation in excised tissue *J. Magn. Reson. Imaging* **8** 1257–65
Carvalhal G F, Smith D S, Mager D E, Ramos C and Catalona W J 1999 Digital rectal examination for detecting prostate cancer at prostate specific antigen levels of 4 ng ml^{-1} of less *J. Urol.* **161** 8359
Catheline S, Wu F and Fink M 1999 A solution to diffraction biases in sonoelasticity: the acoustic impulse technique *J. Acoust. Soc. Am* **105** 2941–50
Dutt V, Kinnick R R, Muthupillai R, Oliphant T E, Ehman R and Greenleaf J F 2000 Acoustic shear-wave imaging using echo ultrasound compared to magnetic resonance elastography *Ultrasound Med. Biol.* **26** 397–400
Fentiman 1997 *Introduction to the Cellular and Molecular Biology of Cancer—The Local Treatment of Cancer?* (Oxford: Oxford University Press) chapter 17
Huang S R, Lerner R and Parker K J 1990 On estimating the amplitude of harmonic vibration from the doppler spectrum of reflected signals *J. Acoust. Soc. Am* **88** 2702–12
Huang S, Lerner R and Parker K 1992 Time domain Doppler estimators of the amplitude of vibrating targets *J. Acoust. Soc. Am* **91** 965–74
Lerner R M, Parker K J, Holen J, Gramiak R and Waag R C 1988 Sono-elasticity: medical elasticity images derived from ultrasound signals in mechanically vibrated targets *Acoustical Imaging* vol 19 *(Proc. 16th Int. Symp.)* (New York: Plenum) pp 317–27
Love A E H 1944 *A Treatise on the Mathematical Theory of Elasticity* (New York: Dover) chapter 13
McAleavey S, Phillips D and Parker K J 1999 Flow techniques, industrial *Wiley Encyclopedia of Electrical and Electronics Engineering* ed J G Webster (New York: Wiley) p 620–7
Muthupillai R, Lomas D J, Rossman P J, Greenleaf J F, Manduca and Ehman R L 1995 Magnetic-resonance elastography by direct visualization of propagating acoustic strain waves *Science* **269** 1854–7
Nightingale K, McAleavey S and Trahey G 2003 Shear wave generation using acoustic radiation force: *in vivo* and *ex vivo* results *Ultrasound Med. Biol.* **29** 1715–23

Obek C, Louis P, Civantos F and Soloway M S 1999 Comparison of digital rectal examination and biopsy results with the radical prostatectomy specimen *J. Urol.* **161** 494–9

Sanada M, Ebara M, Fukuda H, Yoshikawa M, Sugiura N, Saisho H, Yamakoshi Y, Ohmura K and Kobayashi K 2000 Clinical evaluation of sonoelasticity measurement in liver using ultrasonic imaging of internal forced low-frequency vibration *Ultrasound Med. Biol.* **26** 1455–60

Smith J, Lawrence A and Ehman R 1999 3D FFT mode filtering for phase gradient velocity measurements *Review of Progress in Quantitative Nondestructive Evaluation* vol 18B, ed D Thompson and D Chimenti (New York: Plenum) pp 15693–600

Tumen H J and Cohn E M 1965 *Gastroenterology* vol III (London: W B Saunders) chapter 98

Taylor L S, Porter B C, Rubens D and Parker K J 2000 Three-dimensional sonoelastography: principles and practices *Phys. Med. Biol.* **45** 1477–94

Vexler A, Polyansky I and Gorodetsky R 1999 Evaluation of skin viscoelasticity and anisotropy by measurement of speed of shear wave propagation with viscoelasticity skin analyzer *J. Invest. Dermatol.* **113** 732–9

Wu Z, Taylor L S, Rubens D J and Parker K J 2002 Shear wave focusing for three-dimensional sonoelastography *J. Acoust. Soc. Am* **11** 439–66

Yamakoshi Y, Sato J and Sato T 1990 Ultrasonic-imaging of internal vibration of soft-tissue under forced vibration *IEEE Trans. Ultrason. Ferroelectr. Freq. Control* **37** 45–53